Pergamon

Int. J. Heat Mass Transfer. Vol. 38, No. 1, pp. 13–21, 1995

0017-9310/95 $9.50 + 0.00

0017-9310(94)00142-1

Modeling heat and mass transfer in fabrics

K. GHALI, B. JONES and J. TRACY

Institute for Environmental Research, Kansas State University, Seaton Hall, Manhattan, KS 66506, U.S.A.

(*Received* 14 *May* 1993 *and in final form* 17 *May* 1994)

Abstract—A numerical model was developed for simulating the heat and mass transfer in fabrics during the wicking process. The model was applied to two different fabrics, cotton and polypropylene. The model shows that, as the water is wicked through the fabric specimens, two temperature zones are formed. Within each region the temperature gradient is small, but between the regions it is more significant. Unlike the temperature, the variation of the fractional saturation is continuous along the specimens. Experiments were also conducted to obtain the temperature distributions during wicking for the two fabrics and to validate the numerical model.

INTRODUCTION

Heat and mass transfer in a porous medium is a process which occurs in nature and many engineering applications. These applications include agricultural production processes, petroleum extraction, moisture movement in soil and moisture movement in fabrics. The particular application of interest in the present study is the movement of moisture in clothing materials.

The fabrics worn next to the skin have a direct influence on thermal comfort. Unevaporated sweat may be wicked through a fabric that comes into contact with the skin. In addition to altering the mechanical and thermal properties of the fabric, there are energy flows associated with the wicking. This wicking affects the overall heat transfer from the clothed human body and the thermal comfort of the human subject [1].

Numerous models and their solutions of the heat and mass governing equations are present in the literature. Krischer and Rohnalter [2] were some of the first researchers to consider the energy equation in studying the drying process. Later, Philip and Devries [3] developed a set of governing equations using conservation of moisture and thermal energy. Their model improved previous studies in drying by including the capillary flow. Similar governing equations were developed by Luikov [4]. Later, Whitaker [5] developed a theory for drying using a volume-averaged conservation equations which provided more insight into the nature of heat and mass transfer process.

Since the application addressed in this study is fabric, this paper will focus on the work that is related to heat and moisture transfer in fabrics. Henry [6] introduced an analytical model to describe the transient diffusion problem in hygroscopic materials. Henry's model was later improved by Nordon and David [7], who were able to solve the non-linear differential equation of moisture transfer numerically by the finite difference method. Later, Farnworth [1] introduced a model that was able to simulate the transient heat and mass transfer in a multi-layered clothing system. Recently, Jones *et al.* [8] developed a model that can simulate the transient response of clothing and predict the effect of this response on heat flow from the human body.

The above-mentioned models were developed for the vapor moisture transfer through fabric materials and the liquid layer was treated as immobile. The objective of this research is to examine simultaneously both liquid and vapor transfer and their effects on the temperature distribution.

MATHEMATICAL DEVELOPMENT

The structure of wet fabrics consists of the fiber matrix, liquid water, and a gaseous phase of water vapor and air. Predicting the heat and mass transfer in such a system is a difficult task. The problem is complicated by the fact that the transport properties involved are non-linear functions of temperature and moisture content, and that fiber swelling may occur due to changes in the degree of the saturation. This swelling may affect the porosity and the available void space for the liquid and the gaseous mixture transport inside the solid matrix. Because of the complexity of the problem the following approximations are imposed on the transport process.

(1) The fibrous system is represented by an ideal continuum medium and is divided into volume fractions of liquid, solid, and liquid vapor and air mixture at a particular location. The inhomogeneity scale of the three-phase, solid, liquid and gas system is far smaller than the characteristic length over which an appreciable change in moisture content occurs.

(2) The solid phase is considered to be non-deform-

NOMENCLATURE

A	area of the fabric specimen [cm^2]
D	diffusion coefficient of water–air [cm^2 s^{-1}]
g	acceleration due to gravity [cm s^{-2}]
h	capillary pressure head [cm]
H	distance along the specimen [cm]
K	hydraulic conductivity [cm s^{-1}]
N	shape functions
Q	latent heat of evaporation [J g^{-1}]
R	gas constant of the vapor phase [J mole K^{-1}]
S	saturation degree, dimensionless
T	absolute temperature [K]
t	time [s]
C_p	effective volumetric heat capacity [J g^{-1} K^{-1}]
C_{pl}	specific heat of liquid water [J g^{-1} K^{-1}]
C_{ps}	specific heat of the fabric fibers [J g^{-1} K^{-1}]
h_c	heat transfer coefficient [W cm^{-2} °C^{-1}]
h_l	enthalpy of liquid water [J g^{-1}]
h_m	mass transfer coefficient [g s^{-1} cm^{-2} Pa^{-1}]
J_l	mass flux of liquid [g cm^{-2} s^{-1}]
J_v	mass flux of vapor [g cm^{-2} s^{-1}]
K_l	conductivity of liquid water [W cm^{-1} K^{-1}]
K_s	conductivity of the fabric [W cm^{-1} K^{-1}]
P_v	saturated vapor pressure [Pa]
P_∞	ambient vapor pressure [Pa]
T_∞	ambient temperature [K]
$\{\mathbf{S}\}$	saturation vector
$\{\mathbf{T}\}$	temperature vector
$\{\dot{\mathbf{S}}\}$	saturation rate vector
$\{\dot{\mathbf{T}}\}$	temperature rate vector
$[C_s]$	lumped time capacitance of the saturation
$[K_s]$	liquid transfer stiffness matrix
$[K_{vs}]$	vapor transfer stiffness matrix
$\{\mathbf{Q}_m\}$	mass evaporation vector
$\{\mathbf{Q}_g\}$	load drainage vector
$[C_T]$	lumped time capacitance of the temperature
$[K_T]$	conductive stiffness matrix
$\{\mathbf{Q}_T\}$	evaporative vector
$[K_{vT}]$	evaporative stiffness matrix
$[K_{lT}]$	convective stiffness matrix
$[K_{hT}]$	heat transfer stiffness matrix.

Greek symbols

ε	void fraction
ε_l	volume fraction of the liquid phase [cm^3 cm^{-3}]
ε_g	volume fraction of the gaseous phase [cm^3 cm^{-3}]
ρ	effective density of the fabric specimen [g cm^{-3}]
ρ_l	liquid water density [g cm^{-3}]
ρ_v	water vapor density [g cm^{-3}]
δ	fabric thickness [cm]
λ	effective volumetric conductivity [W cm^{-1} K^{-1}].

able. Based on this assumption, mechanical swelling and shrinkage of the solid phase are not included. Some fibers, particularly natural materials, do swell. However, in actual fabrics the fiber is usually a small portion of the total volume. Therefore, any swelling that may occur has a relatively small effect on the void space for moisture movement. Also, experimental data for permeability will reflect the effects of swelling.

(3) Darcy's equation is used to describe the transient flow through the saturated and unsaturated regions in the fibrous medium, since the liquid is flowing at a very low Reynolds number.

(4) There is no convective flow of the vapor–air mixture.

(5) The liquid component is incompressible and the vapor–air mixture is considered to be an ideal gas.

(6) The fiber system, liquid, and gaseous phases of the fibrous media are in local thermodynamic equilibrium.

(7) Compressional work, viscous dissipation and diffusive energy are considered negligible.

(8) The mass concentration of water vapor is small compared to that of liquid water.

Given such approximations, the one-dimensional heat and moisture conservation equations for a fabric specimen whose surfaces are exposed to the environment can be written as

$$\frac{\partial(\varepsilon_l \rho_l)}{\partial t} + \frac{\partial}{\partial z}(J_l) + \frac{\partial}{\partial z}(J_v) + \frac{2h_m}{\delta}(P_v - P_\infty) = 0 \quad (1)$$

$$\rho C_p \frac{\partial T}{\partial t} + J_l \frac{\partial}{\partial z}(h_l) + Q\frac{2h_m}{\delta}(P_v - P_\infty) + \frac{2h_c}{\delta}(T - T_\infty) + Q\frac{\partial}{\partial z}(J_v) = \frac{\partial}{\partial z}\left(\lambda \frac{\partial T}{\partial z}\right). \quad (2)$$

The liquid and vapor fluxes can be described by using the equations of Darcy and Fick:

$$J_l = \rho_l K\left[\frac{\partial h}{\partial S}\frac{\partial S}{\partial z} - 1\right] \quad (3)$$

$$J_v = -\left[\varepsilon_g D \frac{\partial \rho_v}{\partial T}\frac{\partial T}{\partial z}\right]. \quad (4)$$

The thermal conductivity of the fibrous medium includes heat conduction in the liquid, the fiber matrix and the gaseous mixture. The effective thermal con-

ductivity of the water–fiber combination can be written as

$$\lambda = (1-\varepsilon)K_s + S\varepsilon K_l \tag{5}$$

where K_s represents the conductivity of the fabric which includes conductance due to the fibers and due to the gaseous mixture.

The effective heat capacity of the water–fiber combination is written as

$$\rho C_p = (1-\varepsilon)\rho_s C_{ps} + S\varepsilon\rho_l C_{pl}. \tag{6}$$

By substituting equations (3)–(6) into equations (1) and (2), a set of two independent equations that describes the coupled heat and mass transfer in a unit volumetric element of fibrous media is obtained.

$$\frac{\partial S}{\partial t} + \frac{\partial}{\partial z}\left[\frac{K}{\varepsilon}\left(\frac{\partial h}{\partial S}\frac{\partial S}{\partial z} - 1\right)\right] - \frac{\partial}{\rho_l \partial z}\left[(1-S)D\frac{\partial \rho_v}{\partial T}\frac{\partial T}{\partial z}\right] + \frac{2h_m}{\rho_l \delta\varepsilon}(P_v - P_\infty) = 0 \tag{7}$$

$$(\rho C_p)\frac{\partial T}{\partial t} = \frac{\partial}{\partial z}\left[\lambda\frac{\partial T}{\partial z}\right] - Q\frac{2h_m}{\delta}(P_v - P_\infty) - K\left(\frac{\partial h}{\partial S}\frac{\partial S}{\partial z} - 1\right)C_{pl}\frac{\partial T}{\partial z} - \frac{2h_c}{\delta}(T - T_\infty) + Q\frac{\partial}{\partial z}\left[(1-S)\varepsilon D\frac{\partial \rho_v}{\partial T}\frac{\partial T}{\partial z}\right]. \tag{8}$$

The above two equations represent the moisture and energy conservation equations. In order to solve these equations, K, the hydraulic conductivity which defines the ease with which flow passes through the fibrous medium, ε, the porosity, $\partial h/\partial s$, which represents the driving force available to pass the fluid through the fibrous pores, λ, the effective thermal conductivity of the fabric, the boundary heat and mass transfer coefficients, h_m and h_c, and the thickness of the fabric δ are needed.

NUMERICAL SOLUTION

Equations (7) and (8) were solved using the Galerkin finite element method [10]. This method simulates a continuous system as discrete elements with approximate solutions developed for each element. Using Galerkin's method, the solution can be expressed as

$$\sum_{n-1}^{n}\int_l R(z,t)N(z)\mathrm{d}z = 0 \tag{9}$$

where R is the residual between the exact and approximate governing differential equation, N is the shape function which is chosen to be linear in the present study, l is the length of the system, and n is the total number of elements. Using Galerkin's procedure and applying the boundary conditions by using Green's theorem, equations (7) and (8) can be written as

$$[C_s]\{\mathbf{S}\} = [K_s]\{\mathbf{S}\} - [K_{vs}]\{\mathbf{T}\} - \{\mathbf{Q}_g\} - \{\mathbf{Q}_m\} \tag{10}$$

$$[C_T]\{\mathbf{S}\} = -[K_T]\{\mathbf{T}\} - [K_{vT}]\{\mathbf{T}\} - [K_{lT}]\{\mathbf{T}\} - [K_{hT}](T - T_\infty) - \{\mathbf{Q}_T\}. \tag{11}$$

Each of the above variables is defined in the following equations:

$$[C_s] = \sum_{e=1}^{n}\int_l N_i\,\mathrm{d}z \tag{12}$$

$$[K_s] = \sum_{e=1}^{n}\int_l \frac{K}{\varepsilon}\frac{\partial h}{\partial S}\frac{\mathrm{d}N_i}{\mathrm{d}z}\frac{\mathrm{d}N_j}{\mathrm{d}z}\mathrm{d}z \tag{13}$$

$$[K_{vs}] = \sum_{e=1}^{n}\int_l \frac{1}{\rho_l}\left[(1-S)D\frac{\partial \rho_v}{\partial T}\right]\frac{\mathrm{d}N_i}{\mathrm{d}z}\frac{\mathrm{d}N_j}{\mathrm{d}z}\mathrm{d}z \tag{14}$$

$$\{\mathbf{Q}_m\} = \sum_{e=1}^{n}\int_l N_i\frac{2h_m}{\delta\rho_l\varepsilon}(P_v - P_\infty)\,\mathrm{d}z \tag{15}$$

$$\{\mathbf{Q}_g\} = \sum_{e=1}^{n}\int_l \frac{K}{\varepsilon}\frac{\mathrm{d}N_i}{\mathrm{d}z}\mathrm{d}z \tag{16}$$

$$[C_T] = \sum_{e=1}^{n}\int_l (\rho C_p)N_i\,\mathrm{d}z \tag{17}$$

$$[K_T] = \sum_{e=1}^{n}\int_l \lambda\frac{\mathrm{d}N_i}{\mathrm{d}z}\frac{\mathrm{d}N_j}{\mathrm{d}z}\mathrm{d}z \tag{18}$$

$$\{\mathbf{Q}_T\} = \sum_{e=1}^{n}\int_l N_i Q\frac{2h_m}{\delta}(P_v - P_\infty)\,\mathrm{d}z \tag{19}$$

$$[K_{vT}] = \sum_{e=1}^{n}\int_l Q(1-S)\varepsilon D\frac{\partial \rho_v}{\partial T}\frac{\mathrm{d}N_i}{\mathrm{d}z}\frac{\mathrm{d}N_j}{\mathrm{d}z}\mathrm{d}z \tag{20}$$

$$[K_{lT}] = \sum_{e=1}^{n}\int_l K\left(\frac{\partial h}{\partial S}\frac{\partial S}{\partial z} - 1\right)C_{pl}N_i\frac{\mathrm{d}N_j}{\mathrm{d}z} \tag{21}$$

$$[K_{hT}] = \sum_{e=1}^{n}\int_l \frac{2h_c}{\delta}N_i N_j\,\mathrm{d}z. \tag{22}$$

The partial derivative of the saturation and temperature can be approximated using a numerically stable, implicit, backward difference scheme:

$$\frac{\partial S}{\partial t} = \frac{S^2 - S^1}{\Delta t} \tag{23}$$

$$\frac{\partial T}{\partial t} = \frac{T^2 - T^1}{\Delta t} \tag{24}$$

where superscripts are used to indicate time "1", and time "2". Substitution of equations (23) and (24) into equations (10) and (11) gives

$$([C_s] - \Delta t[K_s])\{\mathbf{S}^2\} = [C_s]\{\mathbf{S}^1\} - \Delta t[K_{vs}]\{\mathbf{T}^2\} - \Delta t\{\mathbf{Q}_g\} - \Delta t\{\mathbf{Q}_m\} \tag{25}$$

$$([C_T] + \Delta t[K_T] + \Delta t[K_{hT}] + \Delta t[K_{lT}] + \Delta t[K_{vT}])\{\mathbf{T}^2\} = [C_T]\{\mathbf{T}^1\} - \Delta t\{\mathbf{Q}_T\} + \Delta t[K_{hT}]\{\mathbf{T}_\infty\}. \tag{26}$$

Equations (25) and (26) are non-linear equations and some type of iterative technique is needed to arrive at a solution. The method of successive substitution is applicable for this type of equation. In this approach, information is passed between the two equations iteratively, starting from the initial temperature and saturation conditions. For each time step, the iteration

continues until convergence is reached. To avoid divergence, the information from one equation was damped by using a relaxation factor of 0.1 before passing it to the following iteration.

MODEL VERIFICATION

Untreated interlock knit cotton and spun polypropylene were chosen as representative of commonly used fabrics with extremes in properties related to liquid moisture transport. The cotton fiber is very hydrophilic (small contact angle), whereas polypropylene is hydrophobic (large contact angle). The capillary pressure as a function of saturation was determined by the "long column" test [11]. The hydraulic conductivity as a function of saturation was obtained using the "siphon" and the "transient test" [11]. The porosity of the fabric specimens was measured from the knowledge of the specimen dimensions and the fiber density [11], while the fabric conductivity was determined experimentally using a hot plate apparatus [11]. The mass transfer coefficient at the exposed surface was also measured experimentally at different degrees of saturations for both fabrics (Appendix A). For both specimens the mass transfer coefficient was near zero for saturations below some critical value, and essentially constant at all saturations above this same critical value. The heat transfer coefficient was estimated from knowledge of the saturated mass transfer coefficient by using the Lewis Relation [12].

Also initial and boundary conditions are needed for the solution of equations (7) and (8). For example, the initial condition in the fabric can be expressed

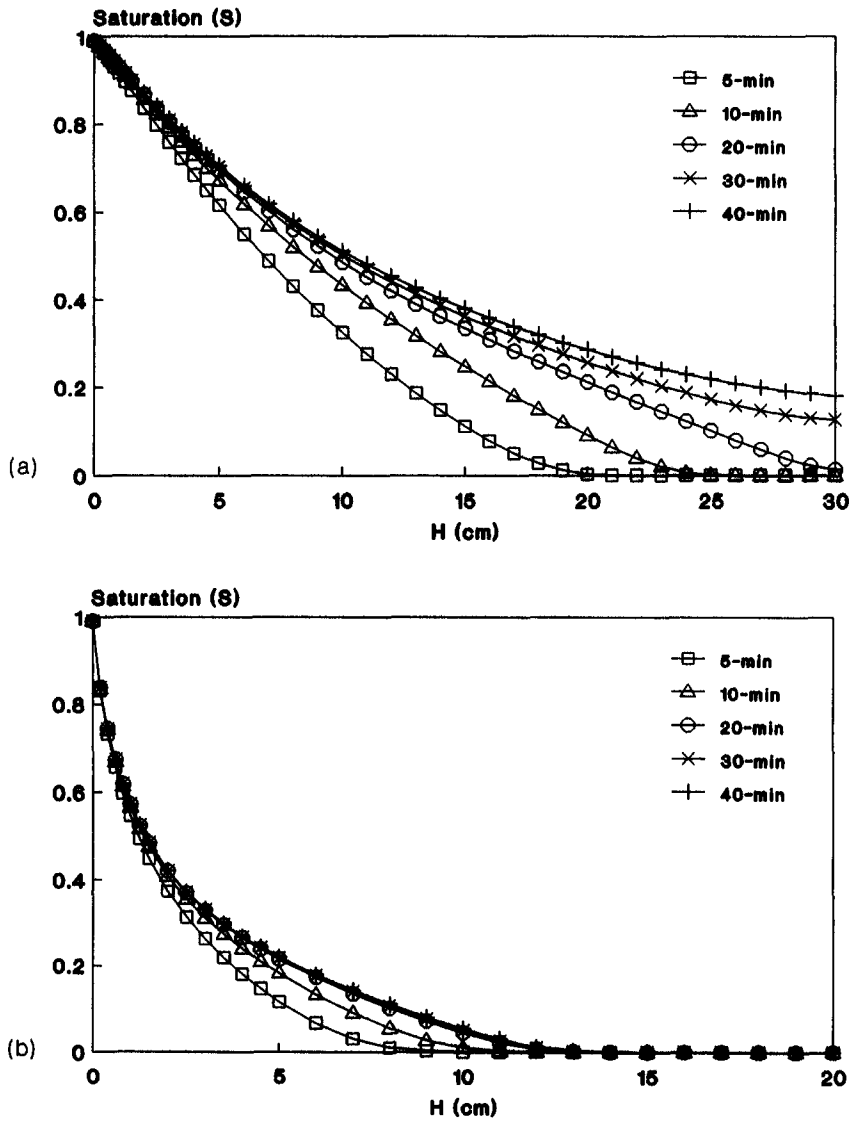

Fig. 1. Model prediction of saturation vs height: (a) cotton samples; (b) polypropylene samples.

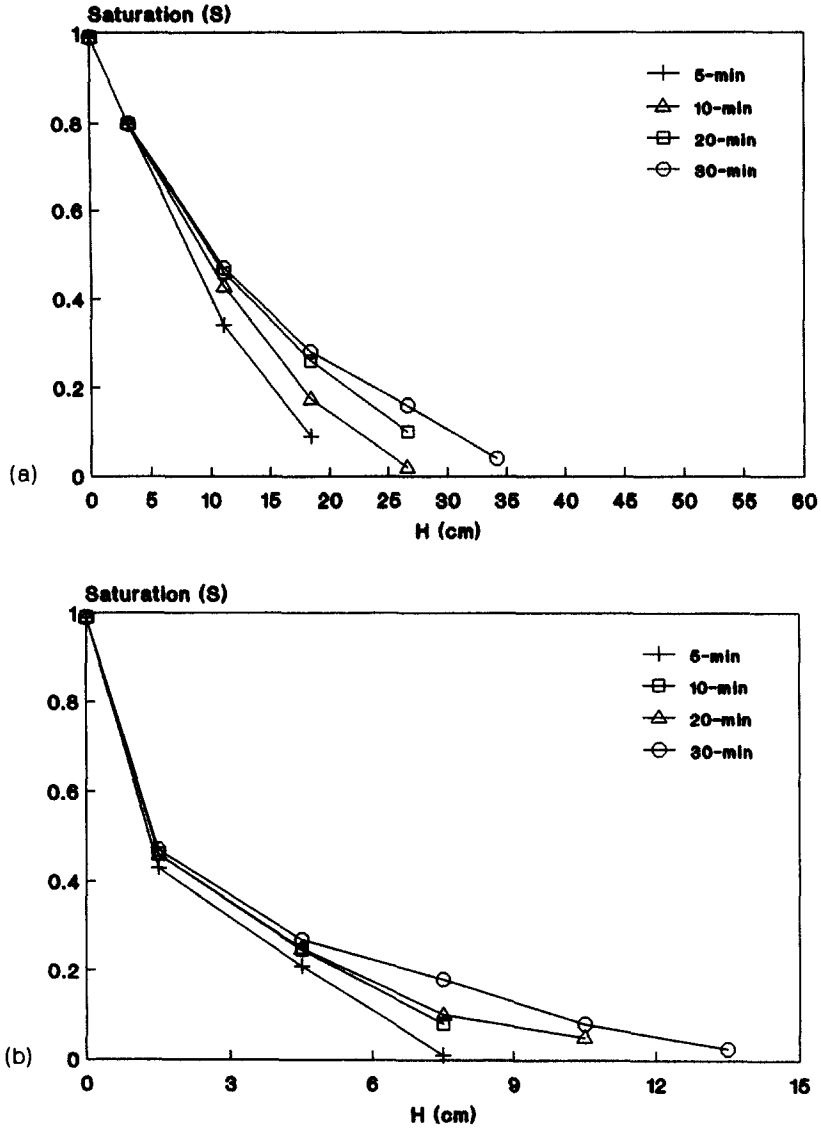

Fig. 2. Experimental measurements of the saturation values vs height: (a) cotton samples; (b) polypropylene samples.

as: $S(z,0) = S_0(z)$, $T(z,0) = T_0(z)$, and the boundary conditions were chosen to be fixed at one end while the other end is a no-flow, adiabatic boundary.

Model predictions show that the liquid saturation varies smoothly along the length of the sample, but increases with time until a steady-state distribution is attained (Fig. 1). In another related study [12], wicking was modeled without including the effects of energy transport. The transient saturation data collected in that study agreed with the model within ± 0.1 (Figs. 1 and 2). Including energy effects in the model has minimal effect on the saturation predictions, at least for moderate conditions. Therefore, additional saturation data are not needed to validate the saturation predictions of the model developed here. However, data to validate the ability of the model to predict the results of energy effects were needed.

Experiments were conducted on the cotton and polypropylene fabrics to measure their temperature distribution during the wicking process. Specimens were cut from different locations in the fabric samples to minimize the effect of any local non-homogeneity that may exist. A small plastic rod with a diameter of 0.6 cm was attached to each end of each specimen. The purpose of these rods was to prevent the specimens from curling up during the test. The tests were conducted in an environmental chamber at an air temperature of 26°C, a relative humidity of 70% and air velocity of 0.2 m s^{-1}. The specimens were suspended over a beaker of distilled water inside the environmental chamber: however, the specimen free end was not in contact with the water. The beaker was sealed by plastic wrapping to minimize any evaporation that might occur. The distilled water and the

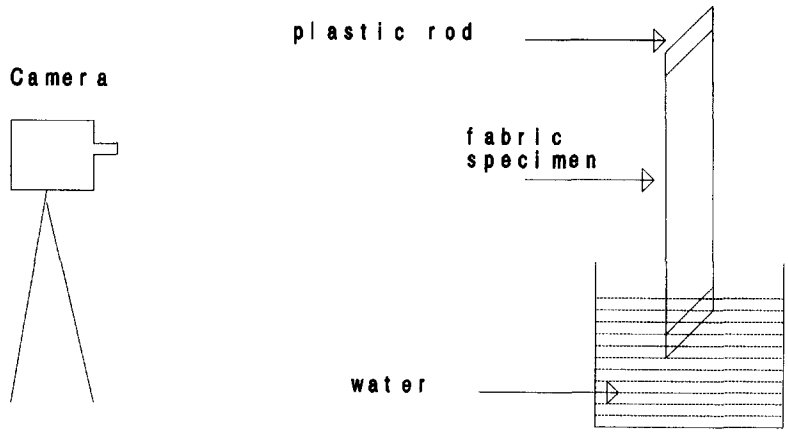

Fig. 3. Temperature measuring experiment.

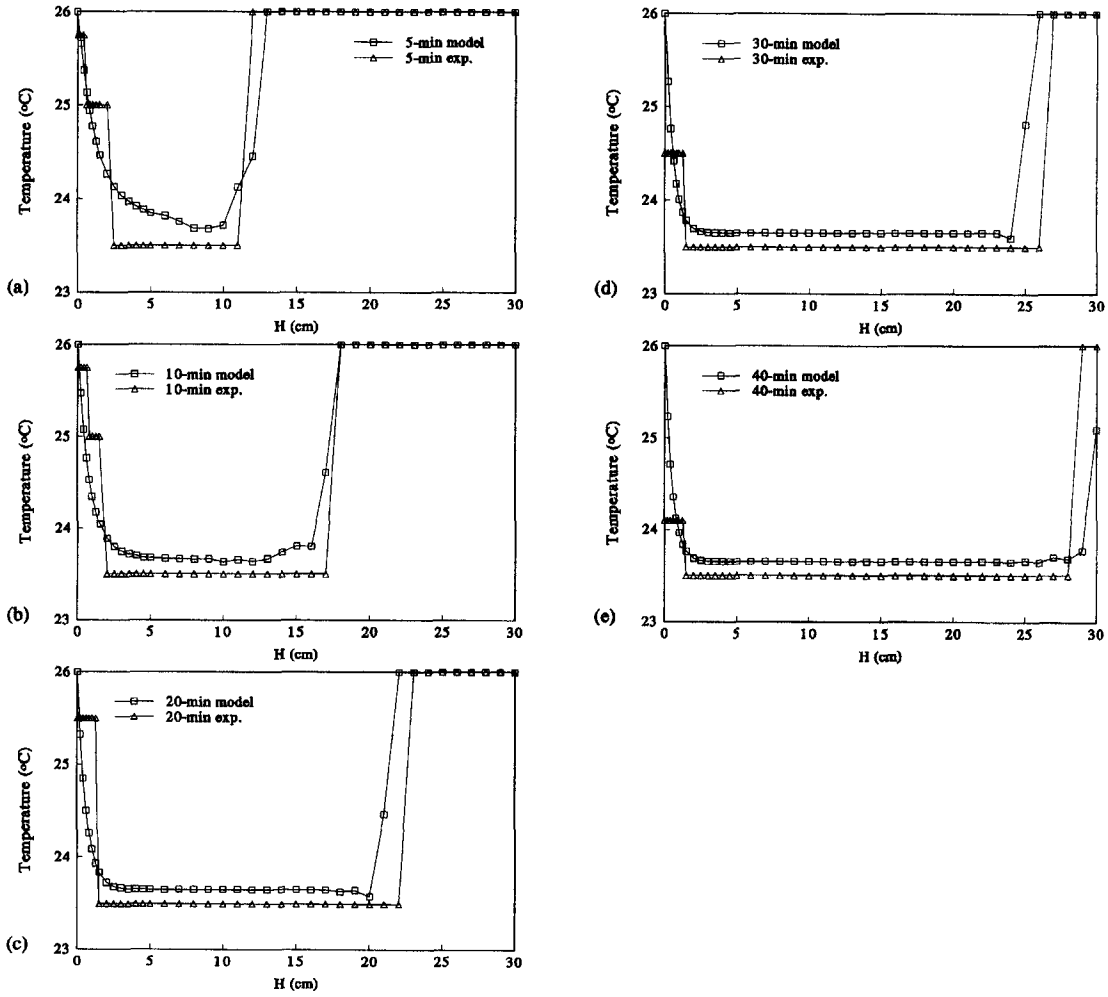

Fig. 4. Comparison of the transient model with the experimental data for the cotton samples: (a) 5 min; (b) 10 min; (c) 20 min; (d) 30 min; and (e) 40 min.

fabric specimen were conditioned inside the environmental chamber for two days prior to testing so that the fabric specimen and the distilled water reached equilibrium with the room conditions. An infrared video camera with a resolution of $\pm 0.5^{\circ}C$ was also placed inside the chamber and was focused on the fabric specimen. This camera provided a means for adjusting the emissivity, which was set at 0.97 for

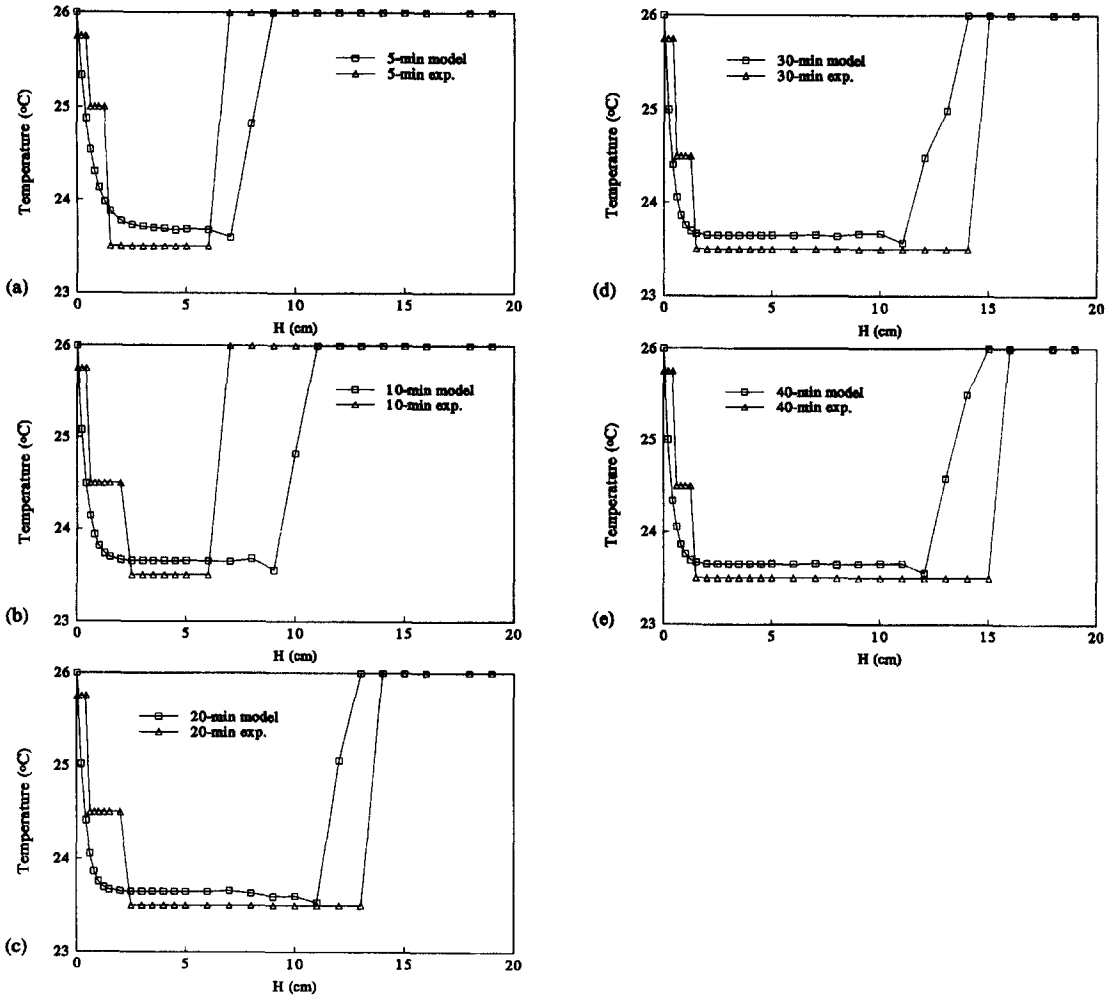

Fig. 5. Comparison of the transient model with the experimental data for the polypropylene samples: (a) 5 min; (b) 10 min; (c) 20 min; (d) 30 min; and (e) 40 min.

the approximate emissivity of the fabric test. At the beginning of the test, the infrared camera was turned on and the plastic wrapping around the beaker was removed. The free end of the specimen was submerged in the distilled water such that the level of water was just at the top of the plastic rod (Fig. 3).

Since the room relative humidity was less than 100%, evaporation occurred at the fabric surface causing the temperature of the fabric to drop below the ambient room temperature. As the water was wicked through the fabric, two temperature zones developed. The temperature gradient within each was negligible, but there was a steep gradient between the two zones. This result was consistent with the mass transfer coefficient measurements discussed previously. Liquid wicked into the fabric increasing the saturation. However, there was essentially no evaporation at a given point until the saturation exceeded a critical value. When that value was exceeded, then evaporation occurred as if the surface were fully wetted. These same results were predicted by the model as presented in Figs. 4 and 5. The location of the temperature front predicted agrees with the experimental results, generally within 2 cm for cotton and 3 cm for the polypropylene. It should be noted that the accuracy of the model predictions of the front location are strongly dependent on the mass transfer coefficients data. The evaporation mass flow was small compared to the wicking mass flow and saturations were not greatly affected by the evaporation. Thus the temperature front location depends almost entirely on the critical saturation required for evaporation to occur, and accurate prediction of the saturation distribution (Appendix B).

CONCLUSION

Energy is transported in four different forms in the wicking process: (1) conduction; (2) diffusion of moisture in the plane of the fabric; (3) convection of liquid in the plane of the fabric; and (4) evaporation of moisture to the atmosphere surrounding the fabric. Each form is addressed in the following with respect

to the experiments conducted in this study. The first form is very small except at the boundary condition where the fabric is in contact with the water because of the low conductivity of the water and fabric. The second form is negligible because of the small temperature changes that exist during the wicking process; the temperature is nearly constant throughout the fabric except at the wetting front where there is a change of about 2°C. The third form is also negligible because the water is transported at a very low Reynolds number except in the initial stage of wetting where the capillary pressure is very high. Finally, the last form is the most dominant.

The numerical model is capable of simulating the temperature distribution of the fabric specimen during the wicking process and it can predict the temperature front. In the initial stage of wetting, the convective energy is high and the water at the beaker temperature is wicked very rapidly into the fabric. As wicking proceeds, the degree of saturation increases, which causes a decrease in the capillary pressure and thus a decrease in the flow rate and the resulting convective energy. When the degree of saturation becomes high enough, the mass transfer coefficient will attain a significant value, causing evaporation of some of the moisture to the atmosphere. This evaporative energy becomes the dominant energy effect causing the temperature of the fabric to decrease except in the region close to the wetted boundary where conduction and convection liquid are significant.

REFERENCES

1. B. Farnworth, A numerical model of combined diffusion of heat and water vapor through clothing, *Textile Res. Inst.* **56,** 653–655 (1986).
2. O. Krischer and H. Rohnalter, Wärmeleitung und dampldiffusion in feuchten gutërn, *VDI-Forschungsh* **402,** 11(B) (1940).
3. J. R. Philip and D. A. Devries, Moisture movement in porous media under temperature gradients, *Trans. Am. Geophys. Un.* **38**(2), 222–232 (1957).
4. A. V. Luikov, Systems of differential equations of heat and mass transfer in capillary-porous body (Review), *Int. J. Heat Mass Transfer* **18,** 1–14 (1975).
5. S. Whitaker, Simultaneous heat, mass and momentum transfer in porous media: a theory of dry. In *Advances in Heat Transfer* (Edited by J. P. Hartnett and T. F. Irvine), Vol 13. Academic Press, New York (1977).
6. P. S. H. Henry, Diffusion in absorbing media, *Proc. R. Soc.* **171A,** 215–241 (1939).
7. P. Nordon and H. G. David, Coupled diffusion of moisture and heat in hygroscopic textile materials, *Int. J. Heat Mass Transfer* **10,** 853–866 (1967).
8. B. W. Jones, M. Ito and E. A. McCullough, Transient thermal response of clothing system, *Proceedings of the International Conference on Environmental Ergonomics*, Austin, Texas, October, pp. 66–67 (1990).
9. J. Bear, *Dynamics of Fluids in Porous Media*, p. 133. American Elsevier, New York (1972).
10. L. J. Segerlind, *Applied Finite Element Analysis* (2nd Edn). Wiley, New York (1984).
11. K. F. Abu-Ghali, Heat and mass transfer in highly porous media, Ph.D. dissertation, Kansas State University, Manhattan, KS (1992).
12. ASHRAE, *Fundamentals of ASHRAE Handbook*. American Society of Heating, Refrigerating, and Air-conditioning Engineers, Inc. (1989).

APPENDIX A

The mass transfer coefficients at the exposed surface were measured for both the cotton and polypropylene fabrics. The measurement, were conducted inside an environmental chamber at an air temperature of 26°C, a relative humidity of 70% and air velocity of 0.2 m s^{-1}. The fabric specimens were cut into rectangular (0.8 × 0.2 m) pieces. At the beginning of an experiment, a fabric piece was submerged in water and its degree of saturation was calculated from the fabric dimensions, the fabric dry weight and the fabric wet weight. The rectangular piece was then placed horizontally over an accurate balance with only one side exposed to the moving air and its weight loss was monitored, as shown in Fig. A1. At the same time thermistors were attached to the surface of the fabric to also monitor its temperature. Knowing the amount of water evaporated, the temperature of the fabric, the chamber temperature and the chamber relative humidity, the mass transfer coefficient was estimated as a function of saturation according to the following equation:

$$W_l = h_m^* A (P_v - \phi P_\infty) \quad \text{(A1)}$$

where W_l is the weight loss, h_m is the mass transfer coefficient, P_v is the saturated vapor pressure of the fabric, P_∞ is the atmospheric vapor pressure and ϕ is the relative humidity of the chamber. The results of the experiment are shown in Table A1.

APPENDIX B

The simulation results showed that including the energy effect had a minimal effect on the saturation predictions and that the temperature distribution was highly dependent on

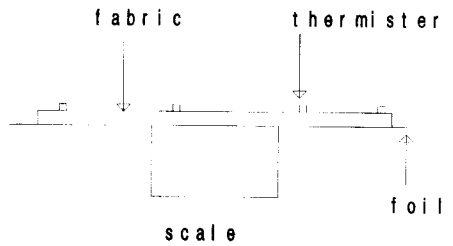

Fig. A1. Mass transfer coefficient measurement.

Table A1. Variation of the mass transfer coefficient with different values of saturation

Polypropylene		Cotton	
S	h_m	S	h_m
0.35	0.018	0.92	0.021
0.28	0.020	0.85	0.022
0.23	0.019	0.78	0.020
0.19	0.018	0.74	0.018
0.11	0.017	0.71	0.019
0.08	0.015	0.61	0.020
0.07	0.002	0.52	0.017
0.03	—	0.27	0.014
		0.22	0.009
		0.16	0.0015
		0.11	—

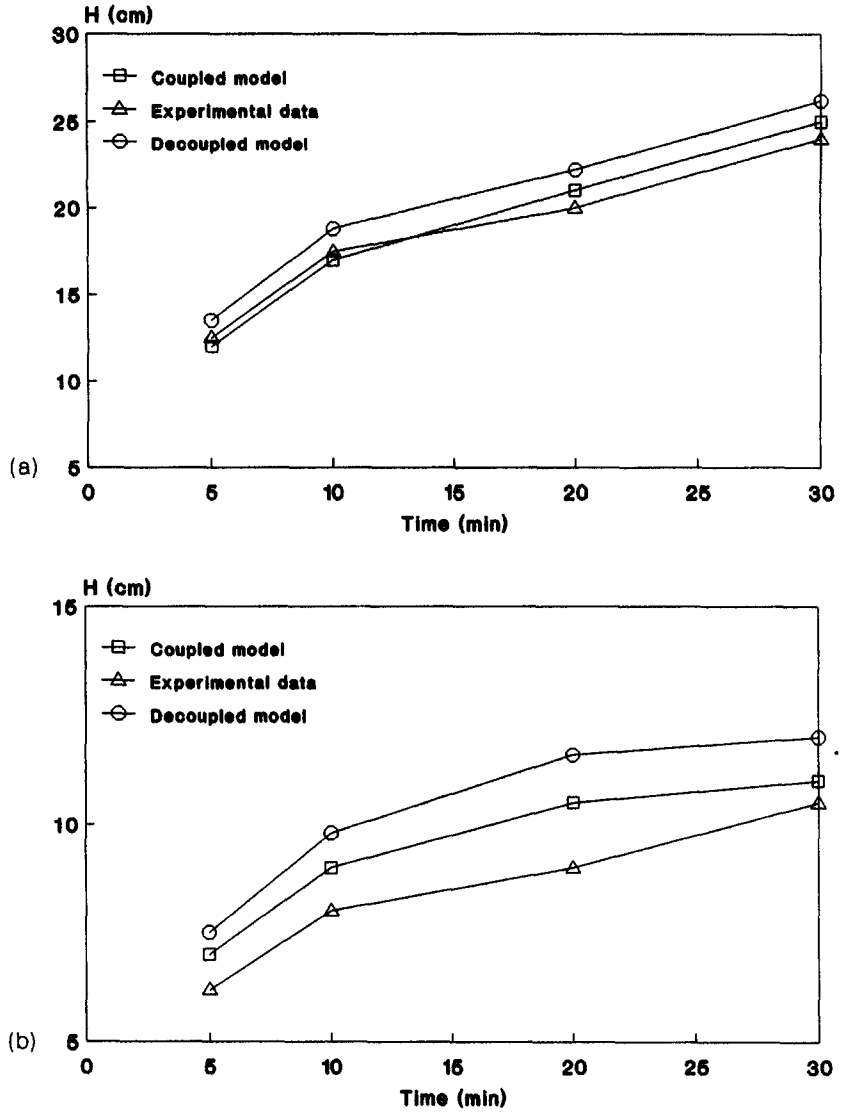

Fig. A2. Critical saturation position vs time: (a) cotton samples; and (b) polypropylene samples.

the mass transfer coefficient, which is a step function of saturation. This could mean that the mass conservation equation could be decoupled from the energy equation and that the temperature distribution could be predicted from the saturation distribution and the position of the critical saturation. In the region above the critical saturation, the temperature of the fabric is expected to be the same as the ambient room temperature, whereas in the region below the critical saturation the temperature of the fabric is expected to be below the ambient room temperature with no temperature gradients, as was discussed earlier.

To examine the dependency of the temperature predictions on the saturation distribution, the simulation model was run without the energy equation and the position of the critical saturation was plotted as a function of time. On the same graph, critical position values obtained from the experimental data and the simulation model with the energy coupled with the saturation equation were also plotted for both fabrics, cotton and polypropylene (Fig. A2). The graph showed that coupling the saturation equation with the energy equation predicts the temperature distribution more accurately than decoupling the two equations.